ADVANCED OPTICAL MATERIALS
www.advopticalmat.de

Nanoscale Optical Display and Sensing Based on the Modification of Fano Lineshape

Jin Xiang, Jingdong Chen, Sheng Lan, and Andrey E. Miroshnichenko**

The shift of Fano resonances has been widely exploited to realize biomedical sensing, optical filtering, and optical switching. Here, the formation of Fano resonances in the scattering spectra of silicon nanoparticles excited by surface plasmon polaritons is reported and the modification of Fano lineshapes is demonstrated. It is revealed that the subradiant and superradiant modes responsible for the formation of Fano resonance originate from the coherent interaction of the electric and magnetic dipoles excited in the silicon nanoparticle with their mirror images induced by a thin metal film. The modification of the asymmetry parameter q can be realized by simply adjusting the angle of the incident light or by slightly varying the environment refractive index. The tuning of the q value is accompanied by the variation of the field enhancement factors and manifested in the color change of the scattered light. The strongest enhancement of both electric and magnetic fields can be achieved at the point of contact between the silicon nanoparticle and the metal film for the symmetric Fano lineshape ($q \approx 0$). These findings indicate the potential applications of such a hybrid metal–dielectric system in sensing, color display, and strong light–matter interaction.

1. Introduction

Fano resonances, typically manifested themselves as asymmetric lineshapes, are a universal phenomenon observed in different branches of physics.[1] Ugo Fano, who provided the first general interpretation for such peculiar profiles, introduced the shape parameter q to account for the ratio of the transition probability to the discrete state and that to the continuum in an atomic system.[2] Since Fano resonances with different spectral features can be fitted by using Fano's formula, the asymmetry parameter q is an important quantity that links the observable far-field signal to the local light–matter interaction taking place at the nanoscale.[1,3–7] As a result, the variation of Fano lineshape has been widely exploited to realize biochemical sensing at the subwavelength scale.[8–14] Benefiting from the rapid development of nanofabrication technology, the manipulation of the Fano resonances in nanoscale structures has become a flourishing field in nanophotonics.[3,4] In particular, plasmonic oligomers are found to be a versatile platform for generating, investigating, and manipulating Fano resonances that provide significant enhancement in both electric and magnetic fields.[15–17] However, plasmonic nanostructures suffer from severe dissipative losses in the visible light spectrum, leading to the Fano resonances with low-quality factors.

In recent years, optically resonant dielectric nanostructures have been demonstrated to be a more promising platform to engineer low-loss Fano resonances.[18–22] More importantly, the coexistence of electric dipole (ED) and magnetic dipole (MD) resonances in a single dielectric nanoparticle offers the opportunity to manipulate the coherent interplay between them that has already inspired all-dielectric-based solutions to directional scattering[23–25] and metasurfaces for efficient wavefront control and beam shaping.[26] Such a dielectric nanocavity can also be integrated with a plasmonic substrate that offers additional degrees of freedom to manipulate the optical response of a hybrid system,[27–33] similar to their plasmonic counterparts.[34] So far, the methods used to modify the spectral features of the Fano resonances in both plasmonic and dielectric systems rely mainly on the geometrical deformation during the fabrication process[18,19,35] and the modification of dielectric environment.[11,36–38] A few strategies for manipulating the lineshapes of Fano resonances have been reported, such as applying uniaxial mechanical stress,[39] femtosecond-laser-induced reshaping of oligomers,[40] and the employment of the Mueller matrix formalism.[41]

The spectral lineshape of an optical Fano resonance is determined by the asymmetry parameter q that encodes the phase shift between the involved subradiant (dark) and superradiant

Dr. J. Xiang, Prof. S. Lan
Guangdong Provincial Key Laboratory of Nanophotonic Functional Materials and Devices
School of Information and Optoelectronic Science and Engineering
South China Normal University
Guangzhou 510006, P. R. China
E-mail: slan@scnu.edu.cn
Dr. J. Chen
College of Physics and Information Engineering
Minnan Normal University
Zhangzhou 363000, P. R. China
Prof. A. E. Miroshnichenko
School of Engineering and Information Technology
University of New South Wales
Canberra, ACT 2600, Australia
E-mail: andrey.miroshnichenko@unsw.edu.au
The ORCID identification number(s) for the author(s) of this article can be found under https://doi.org/10.1002/adom.202000489.

DOI: 10.1002/adom.202000489

(bright) modes. In nanophotonics, it is very difficult to change the resonant frequency of the nanocavity (subradiant mode) without modifying the geometric parameters to acquire such a phase shift.[42] As an alternative, shifting the superradiant mode while fixing the subradiant mode could be an effective way to modify the lineshape of the Fano resonance.

In this article, we show both numerically and experimentally the modification in the lineshape of a Fano resonance in the visible light spectrum realized by exploiting the sensitivity of the surface plasmon polaritons (SPPs) to the angle of the incident light or the refractive index of the environment. We reveal that the Fano resonance arises from the destructive interference between the subradiant and superradiant modes, which originate from the substrate-induced interaction of the ED and MD excited in a high-index dielectric nanoparticle. In particular, we experimentally demonstrate that effective manipulation of Fano lineshape[43] can be realized within 2° change of the incidence angle or with 0.2% change of the environment refractive index, leading to a noticeable color change of the scattering light. We find that the field enhancement factors depend strongly on the lineshape of the Fano resonance, and the largest one is achieved at the symmetric lineshape. The modification of Fano lineshapes opens new horizons for engineering the optical responses of hybrid dielectric-metal systems and for controlling light–matter interaction at the nanoscale, implying potential applications in channel-drop flitters, nanosensors, nanodisplayers, and other novel photonic devices.

2. Results and Discussion

The hybrid dielectric-metal system proposed in this work to demonstrate the modification of Fano lineshape is composed of a spherical silicon (Si) nanoparticle or nanosphere (NS) placed on a thin gold (Au) film, which is the analogue of the channel-drop filter based on photonic bandgap structure.[42] The Si nanoparticles used in this work were fabricated by femtosecond laser ablation (see Experimental Section; Figure S1, Supporting Information) and they were randomly distributed on an Au/SiO_2 substrate with a 50 nm-thick Au film. **Figure 1** schematically shows the excitation of a Si NS by using the SPPs generated on the surface of the Au film, the ED (p_x) and MD (m_y) excited in the Si NS, and their mirror images (p_{xm} and m_{ym}) induced by the Au film.

Based on the mirror image theory,[27] p_x and p_{xm} are antiparallel while m_y and m_{ym} are parallel. As a result, the coherent interaction of p_x and p_{xm} leads to the formation of a narrow mode that is subradiant. In contrast, a broad and superradiant mode is obtained owing to the coherent interaction of m_y and m_{ym}.[28,31] Gap modes are also expected to exist in the gap region between the Si NS and the Au film. However, their contributions to the total scattering are negligible. It is because that the increase of the gap width, which leads to the weakening and eventually the disappearance of the gap modes, does not change so much the total scattering intensity (Figure S2, Supporting Information).

In our case, the SPPs generated on the surface of the Au film act as the excitation source for the Si NS. Although it is a localized wave, it can be scattered into far field by the ED and

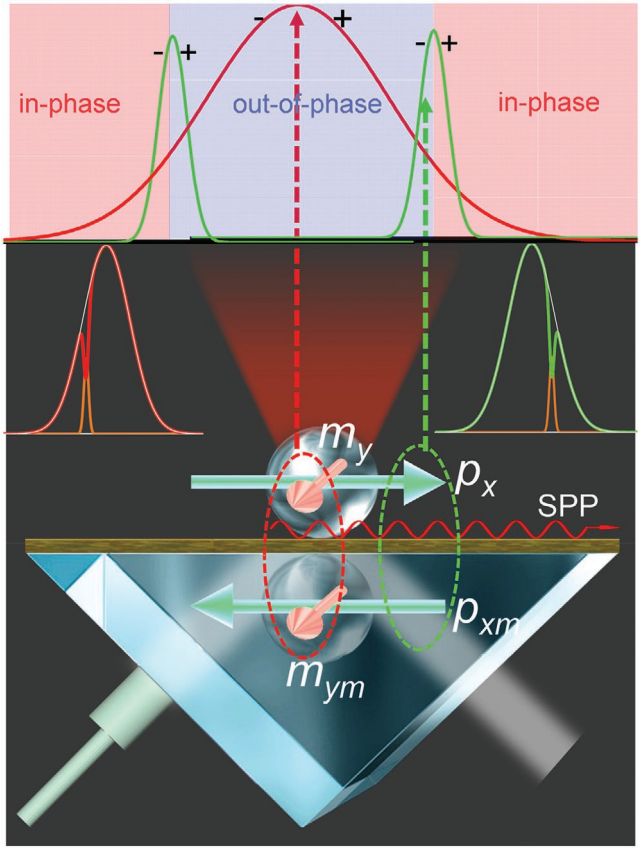

Figure 1. Formation of Fano resonance in the scattering spectrum of a Si NS excited by SPPs. The upper panel illustrates the relative locations of the broad/superradiant and narrow/subradiant modes and the phase relationships between them in different spectral regions. The middle panel presents the Fano lineshapes resulting from the interference of the broad and narrow modes with different relative locations. The lower panel shows schematically the SPPs generated on the surface of an Au film in a total internal reflection configuration, the ED (p_x) and MD (m_y) excited the Si NS, and their mirror images (p_{xm} and m_{ym}) induced by the Au film.

MD excited in the Si NS. As schematically shown in Figure 1, the scattering spectrum of the Si NS is eventually determined by the interference of the resulting subradiant and superradiant modes that generates a Fano resonance. While the subradiant mode arises from the coherent interaction of p_x and p_{xm}, the superradiant mode originates from the coherent interaction of m_y and m_{ym}, which can be readily modified by the excitation source (i.e., the SPPs). It should be emphasized that the simultaneous excitation of ED and MD modes in the Si NS and the introduction of their mirror images via the Au film make it possible to create a Fano resonance in the scattering spectrum. For metallic nanoparticles that support ED modes only, no Fano resonances were observed in their scattering spectra under the excitation of SPPs.[34,44] In Figure 1, we present the phase relationship between the subradiant and superradiant modes in different spectral regions when the subradiant mode is located on the left and right sides of the superradiant one. The Fano resonances formed by the interference between the two modes are also shown. It is apparent that the Fano lineshape can be modified when the subradiant mode is shifted from the left

side across the superradiant mode to the right side, similar to that demonstrated in the photonic bandgap structure.[42]

As mentioned above, one way of modifying the Fano lineshape is to shift the subradiant mode relative to the superradiant one. Since the subradiant mode originates from the coherent interaction of p_x and p_{xm}, its resonant wavelength is determined mainly by the separation between p_x and p_{xm}, which is equal to the diameter of the Si NS. For this reason, the shift of the subradiant mode can only be realized by changing the diameter of the Si NS. In **Figure 2**, we show the scattering spectra measured for Si NSs with different diameters ranging from 150 to 200 nm. The light incidence angle, which governs the resonant wavelength of the superradiant mode (for the reason explained below), was fixed at 46°. It can be seen clearly that the Fano lineshape is modified gradually when the diameter of the Si NS is increased, quite similar to the modification of the Fano lineshape realized in the channel drop filter.[42] In order to characterize more quantitatively the modification of the Fano lineshape, we have fitted the scattering spectra by using the Fano formula and extracted the asymmetric parameters for all the lineshapes, as shown in Figure 2. In this case, the q value varies from –0.30 to 0.47. From the images of the scattered light recorded by using a charge-coupled device (CCD), it is clear that the color of the scattered light remains nearly unchanged because it is mostly determined by the superradiant mode,

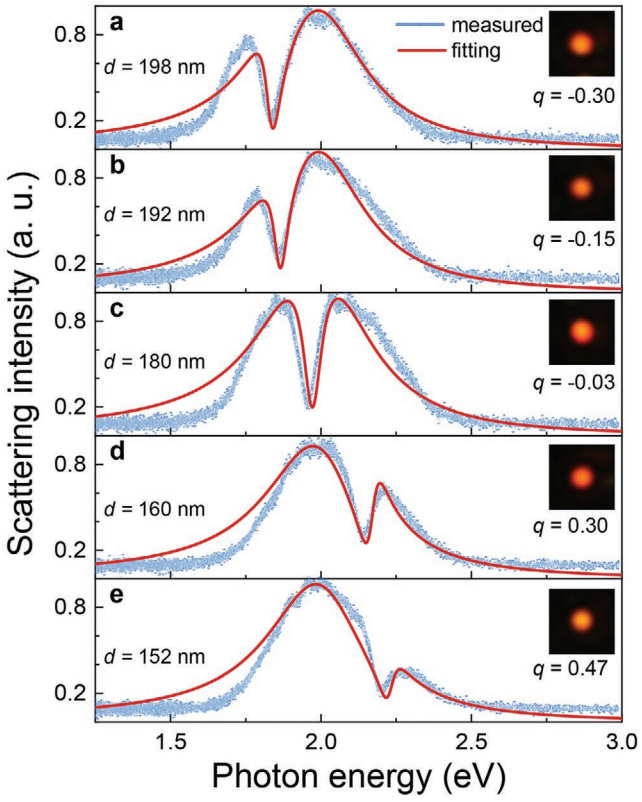

Figure 2. Static manipulation of the Fano lineshape. a–e) Scattering spectra of Si NSs with different diameters (d = 198, 192, 180, 160, and 152 nm) excited by using the SPPs generated on the surface of the Au film. The fitting of the scattering spectra and the extracted q parameters are also presented. The CCD images of the scattering light are shown in the insets.

which was not shifted in this case. Although the tuning of the q value can be achieved by varying the size of the Si NS, similar modifications have been demonstrated in many dielectric and metallic nanostructures.[19,40]

In order to realize an active modification of the Fano lineshape useful for practical applications, the best way is to change only the excitation conditions for a specified Si NS. It implies that the resonant wavelength of the subradiant mode is fixed because it depends only on the size of the Si NS. Therefore, the only way to change the Fano lineshape is to shift the superradiant mode.

Physically, the subradiant mode produces negligible far-field radiation. So, it is not affected by the spectrum of the excitation source, which is the SPPs excited on the surface of the Au film. In sharp contrast, the superradiant mode is a bright one and its radiation can be strongly modified by the excitation source. This unique feature offers us an opportunity for shifting the superradiant mode through the change of the excitation source that is the SPPs generated on the surface of the Au film.

It is well-known that the SPPs on the surface of the Au film can only be excited by using a p-polarized light. Since the SPPs are strongly localized on the surface of the Au film (Figure S3, Supporting Information), they can only be characterized by measuring the spectrum of either the reflected light or the scattered light. In **Figure 3**a,b, we present the spectra simulated and measured for the reflected light in the total internal reflection configuration, which are related to the spectra of the SPPs generated at different incidence angles. It indicates that the resonant wavelength of the SPPs can be readily tuned by simply varying the incidence angle above the critical one.

Alternatively, the spectrum of the SPPs can be extracted by measuring the scattering spectrum of a nanoparticle located on the Au film. Here, a polystyrene (PS) NS with a diameter of 200 nm, which exhibits no resonances in the visible to near-infrared spectral range, was used in the experiment (Figure S4, Supporting Information). The normalized scattering spectra simulated and measured for a PS NS with d ≈200 nm are shown in Figure 3c,d, respectively. It can be seen that the resonant wavelength and linewidth of the SPPs obtained in the scattering spectra match well with the reflection spectra, verifying the feasibility of this method. In Figure 3, the most remarkable feature is the wide tunability and large sensitivity of the SPPs on the incidence angle. It is noticed that the resonant wavelength of the SPPs can be continuously tuned for nearly 200 nm (from 720 to 550 nm) when the incidence angle is varied only 6° (from 45° to 51°). The change of the SPP wavelength is clearly manifested in the variation of the scattering light color, as shown in the inset of Figure 3d. This simple experiment indicates that the radiation of the superradiant mode of a nanoparticle (e.g., the Si NS studied in this work), which exhibits a broad linewidth (i.e., without obvious resonance), can be modified by the SPPs used to excite the nanoparticle. In other words, the superradiant mode of the Si NS can be shifted by modifying the SPP wavelength through the change of the incidence angle.

In our case, the SPPs on the surface of the Au film can be excited when the incidence angle exceeds a critical value of 43°. For smaller incidence angles, no SPPs are generated and the Si NS is excited directly by the transmitted wave on the surface

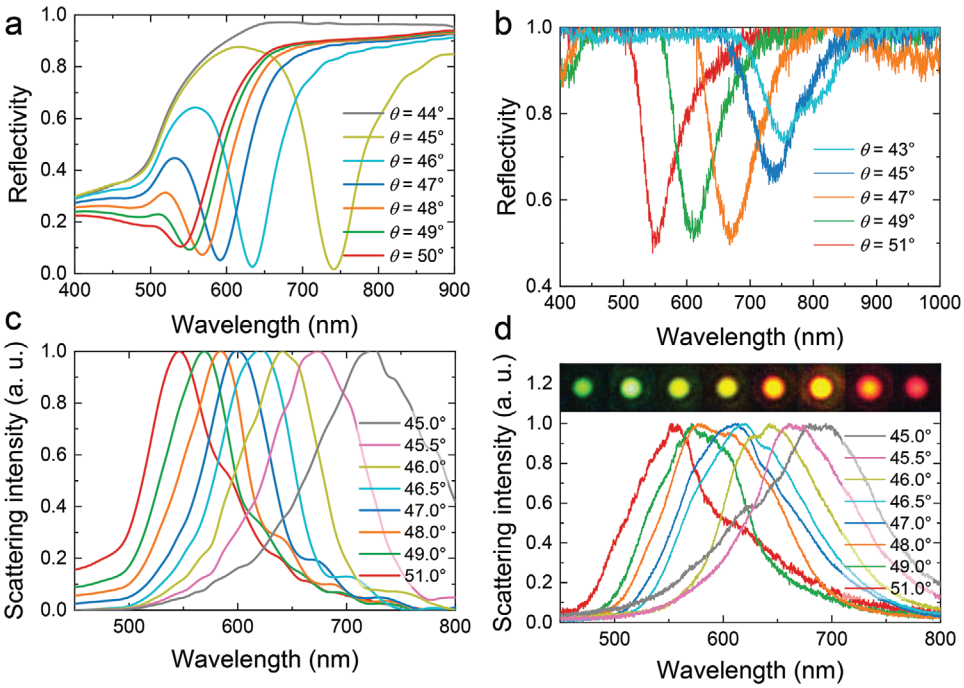

Figure 3. Manipulating of the SPPs. Reflection spectra a) calculated and b) measured for different angles of the incident light used to excite the SPPs on the surface of the Au film. Scattering spectra c) calculated and d) measured for a PS NS with $d = 200$ nm used to scatter the SPPs generated on the surface of the Au film. The CCD images of the scattering light observed at different incidence angles are shown in the insets.

of the Au film (Figure S5, Supporting Information). In this case, the scattering of the Si nanoparticle is quite similar to that described in the previous study where the mirror image theory was first employed to interpret the backward scattering of a Si nanoparticle placed on a metal film.[27] In **Figure 4**a, we show the scattering spectra measured for the Si NS with $d \approx$ 180 nm at three different incidence angles smaller than the critical angle. In this case, only a sharp resonant mode, which arises from the interference of p_x and p_{xm}, is observed in the scattering spectrum.[32] The variation of the incidence angle has little influence on the spectral shape. As shown in Figure 4b, a dramatic change in the scattering spectrum is observed when the incidence angle becomes larger than the critical one. A Fano dip was created at ≈600 nm in the scattering spectrum, and it did not change with the incidence angle.

Here, we employed the SPPs generated on the surface of the Au film to excite the Si nanoparticle. Since the resonant wavelength of the SPPs can be easily adjusted by the incidence angle, the resonant wavelength of the superradiant mode, which originates from the coherent interaction of the MD and its mirror image, can be readily manipulated because the SPPs are scattered into far field mainly by the superradiant mode. The amplitude and phase of the superradiant mode are modified accordingly with its resonant wavelength so that a strong interaction between the subradiant and superradiant modes can be realized.[28] As a result, a pronounced Fano resonance can be created in the scattering spectrum of the Si nanoparticle. In addition, the Fano lineshape, which is sensitive to the incidence angle and the environment refractive index, can be easily modified. More interestingly, the enhancements in electric and magnetic fields are strongly correlated with the Fano lineshape that can be easily manipulated, as demonstrated later. In Figure 4c, we present the scattering spectra of hundreds of Si NSs with different diameters measured by using conventional dark-field microscopy with an incidence angle of 33° at which no SPPs are excited.[32] It can be seen that the sharp resonant mode is red-shifted to longer wavelengths with increase in the diameter of the Si NS. Accordingly, the scattered light color varies from green to red, as shown in the inset. In comparison, the scattering spectra of hundreds of Si NSs with different diameters excited directly by the SPPs are presented in Figure 4d. In each case, the incidence angle was intentionally chosen so that the symmetric Fano lineshape is obtained. Therefore, the incidence angles for measuring the scattering spectra are different for different Si NSs. Similarly, the scattering light color varies from green to red with increase in the diameter of the Si NS.

In Figure 4b, it is interesting to notice that the Fano lineshape of a Si NS with $d \approx 180$ nm can be modified by simply changing the incidence angle, as predicted in the above analysis. It can be seen that the relative intensities of the two scattering peaks can be manipulated and the apparent color can be changed from green to red by simply varying the incidence angle (Figures S6 and S7, Supporting Information). It is remarkable, that the location of the subradiant mode (indicated by the Fano dip) remains unchanged, in good agreement with our theoretical predictions. We also compared the scattering spectra and electric field distributions for two incidence angles, which are smaller and larger than the critical one (Figure S8, Supporting Information). In the former case, the mirror image theory can nicely be employed to reproduce the scattering spectrum and electric field distribution. In the latter case, the formation of a mirror-image-induced MD is clearly manifested in

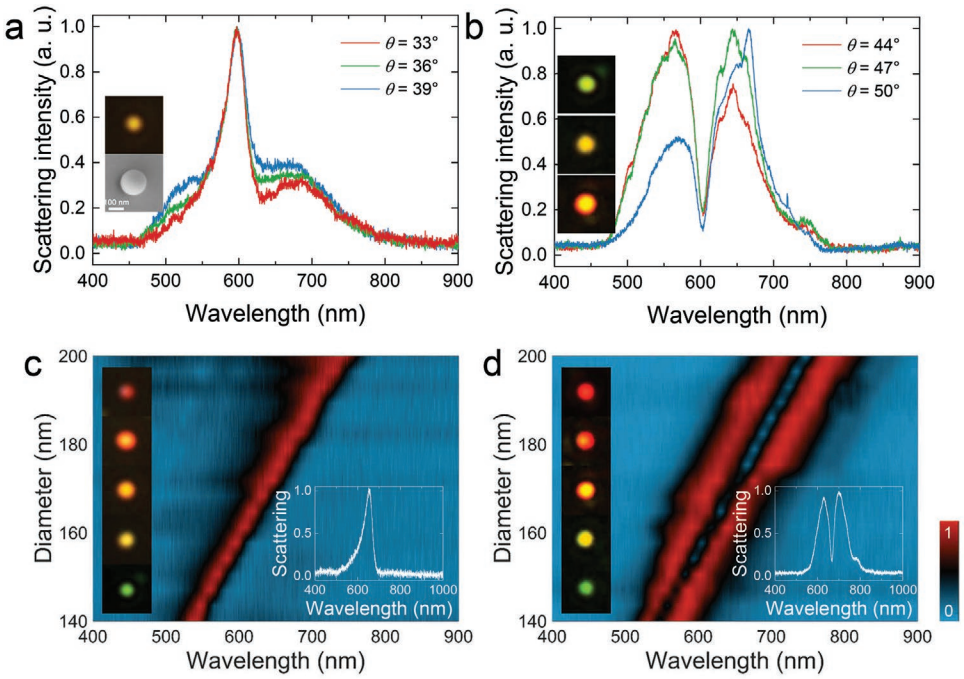

Figure 4. Fano resonances formed in the scattering spectra of Si NSs. Forward scattering spectra measured for a Si NS with $d \approx 180$ nm at three different incidence angles a) smaller and b) larger than the critical angle for total internal reflection. The SEM image of the Si NS and the CCD images of the scattering light are shown in the insets. Evolution of the scattering spectrum and scattering light with increasing diameter of the Si NS measured at incidence angles of c) $\theta = 33°$ and d) $\theta > 43°$. In each case, a typical scattering spectrum is shown in the inset.

the magnetic field distribution on the *XY* plane (on the surface of the Au film).

In order to quantitatively characterize the modification of the Fano resonance, we systematically investigated the evolution of the scattering spectrum with decreasing incidence angle by using another Si NS with $d \approx 188$ nm, as shown in **Figure 5**a. It can be seen that each scattering spectrum can be fitted quite well by the modified Fano formula[45] with appropriate parameters (see Experimental Section; Tables I and II, Supporting Information). As the incidence angle is reduced from 50° to 47.2°, the q parameter is reduced from a negative value to zero. A further reduction in the incidence angle leads to a

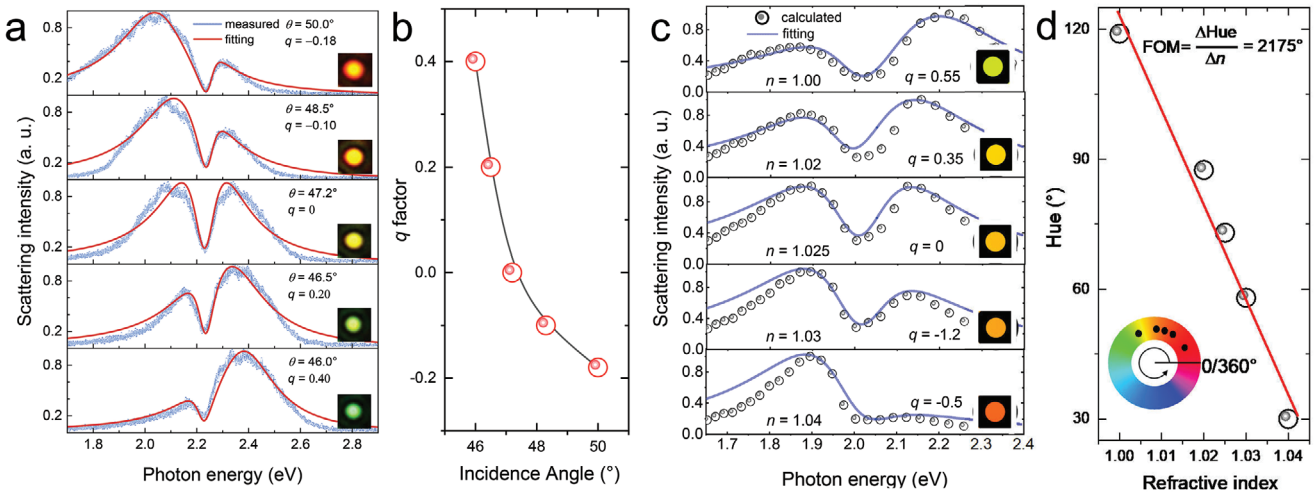

Figure 5. Sensing based on the modification of Fano lineshape. a) Five typical Fano resonances observed in the scattering spectra of a Si NS with $d \approx 188$ nm excited by the SPPs at different incidence angles. The fittings of the scattering spectra and the extracted q parameters are presented. The CCD images of the scattering light are also shown in the insets. b) Dependence of the q value on the incidence angle. c) Evolution of the scattering spectrum with increasing environment refractive index simulated for a Si NS with $d = 188$ nm at an incidence angle of 47°. The fittings of the scattering spectra and the extracted q parameters are presented. The scattering light colors calculated based on the scattering spectra are shown in the insets. d) Dependence of the polar coordinate of the LCHab space (i.e., hue) measured in degrees (modulo 360) on the environment refractive index.

positive value for the q parameter. For clarity, the dependence of the q value on the incidence is presented in Figure 5b. From the fitting results, the resonant wavelength of the subradiant mode is nearly unchanged while the superradiant one is shifted accordingly within 4° variation of the incidence angle, indicating the effectiveness of utilizing the sensitivity of the SPPs on the incidence angle (Figure S9, Supporting Information).

Apart from the incidence angle, it is interesting to find that the Fano lineshape is extremely sensitive to the refractive index of the environment in which the Si NS is embedded, because the SPP wavelength is quite sensitive to the small change of the environment refractive index when the incidence angle is fixed, especially for incidence angles close to the critical one (Figure S10, Supporting Information). Even for a large incidence angle of 47° far from the critical one (43°), a small variation of the environment refractive index from 1.00 to 1.02 can lead to an obvious change in the Fano lineshape, which is also manifested in the extracted q value (see Figure 5c). A further increase of the environment refractive index to 1.04 results in the change of q from 0.55 to –0.5. More interestingly, such a modification in the q parameter originating from a tiny variation of the environment refractive index is clearly reflected in the change of the scattering light (see the inset of Figure 5c), making it attractive for the practical applications in nanoscale sensors. In Figure 5d, we present the dependence of the polar coordinate of the LCHab space (i.e., hue) measured in degrees (modulo 360) on the environment refractive index.[17] Apparently, a linear relationship between the two quantities is observed. The slope of the linear relationship, which is estimated to be $|\Delta\text{hue}/\Delta n| = 2175°$, is the figure of merit (FoM) commonly used to characterize the sensitivity of sensing performance. Surprisingly, it is found that the FoM is one order of magnitude larger than the plasmonic sensors that utilize the Fano resonances generated in oligomers of metallic nanoparticles.[17] In fact, the sensitivity of the q value on the environment refractive index can be one order of the magnitude higher at a smaller incidence angle of 45.5° because the SPP wavelength becomes more sensitive to the incidence angle when it approaches the critical one. In this case, the change in Fano lineshape can be resolved for an environment refractive index change as small as 0.002 and the change of q from 0.25 to –0.22 is observed when the environment refractive index is varied from 1.000 to 1.006 (Figure S10b, Supporting Information).

In general, it is expected that significantly enhanced electromagnetic field can be achieved at the Fano resonance. In **Figure 6**a,b, we present the enhancement factor spectra for the electric (E_x/E_{x0}) and magnetic (H_y/H_{y0}) fields calculated for the Si NS with d = 180 nm. In each case, the maximum

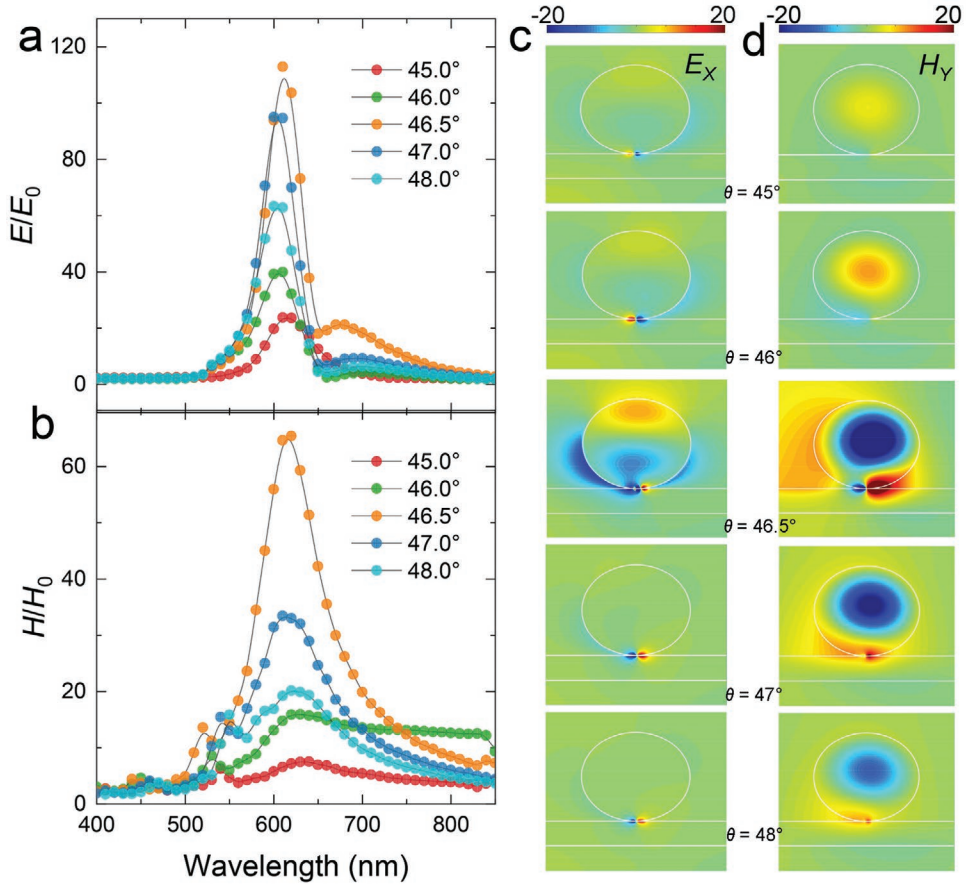

Figure 6. Enhancement of the electric and magnetic fields at the Fano resonance. Enhancement factors for a) electric and b) magnetic fields calculated for the Si NS with d = 180 nm at different incidence angles. The electric and magnetic field distributions (E_x/E_{x0} and H_y/H_{y0}) on the XZ plane are shown in (c) and (d), respectively.

enhancement factor is indeed observed around the Fano dip. More interestingly, it is remarkable that the maximum enhancement factor as large as ≈120 for the electric field (≈65 for the magnetic field) is achieved for the symmetric lineshape (i.e., $q = 0$), which is obtained at an incidence angle of 46°. These values are much larger than those reported previously[31,46] and are quite important for realizing novel photonic devices such as nanosensors and nanolasers. It can be seen that the enhancement factor begins to decrease when the absolute value of the q parameter is increased (i.e., the lineshape becomes more asymmetric). As shown in Figure 6c,d, the in-plane component of the electric field (E_x and H_y) can be controlled by simply varying the incidence angle. This unique feature offers us the opportunity to control the coupling strength between the excitons in a 2D material and the SPPs, making it possible to manipulate the Rabi splitting observed in the scattering spectrum. It is remarkable that the $q \approx 0$ appearing in the Fano lineshape is accompanied by an obvious phase change in E_x and H_y when the superradiant mode is shifted across the subradiant one, shown in Figure 6c,d. As the Fano resonance observed in such hybrid system relies on the excitation of SPPs, it implies that we can switch off the Fano resonance by changing the polarization of the incident light from *p*- to *s*-polarization (Figure S11, Supporting Information), providing another degree of freedom for controlling the scattering of SPPs by using Si NSs.

It is expected that the interaction between the Si nanoparticle and the metal film can be further enhanced by replacing the Au film used in this study with a silver (Ag) film, which possesses a smaller Ohmic loss in the visible light spectrum. We calculated the scattering spectra of a Si nanoparticle (d = 200 nm) placed on an Ag film and excited by the SPPs. It can be seen that the reversal of the asymmetric parameter q can be realized by slightly varying the incidence angle from 45.2° to 45.3°. As compared with the Si nanoparticle placed on the Au film (see Figure 5a), the sensitivity of the Fano lineshape to the incidence angle is further improved. In addition, a larger electric field enhancement factor of ≈170 is achieved at the contacting point between the Si nanoparticle and the Ag film, which is more useful for realizing strong light–matter interaction. Moreover, the Fano lineshape becomes more sensitive to the change in the environment refractive index, making it possible for sensing some vapors with large refractive indices or vapors with high pressures (see Figure S12, Support Information).

3. Conclusion

In summary, we have predicted theoretically and demonstrated experimentally the modification of the Fano resonance formed in the scattering spectrum of spherical Si nanoparticles by exploiting the sensitivity of the SPPs on the incidence angle and environment refractive index. It is revealed that the Fano dip originates from the destructive interference between the subradiant and superradiant modes that originate from the coherent interaction between ED and MD with their mirror images, respectively. We showed that the effective manipulation of Fano lineshape can be realized by simply adjusting the incidence angle or slightly changing the environment refractive index. Such q-parameter reversal is generally accompanied by the change of the vivid scattering light color from green to red. We found that the largest enhancement factor of ≈120 for the electric field (≈65 for the magnetic field) is achieved for the symmetric lineshape and the manipulation of the Fano lineshape opens new horizons for controlling the in-plane electric and magnetic fields. Our findings might facilitate the design of novel photonic devices, such as demultiplexers, biosensors, displayers, and nanolasers in the integrated optical systems.

4. Experimental Section

Sample Preparation: Si NSs with diameters ranging from 100 to 250 nm were fabricated by using femtosecond laser ablation. A femtosecond laser amplifier (Legend, Coherent) with a pulse duration of 100 fs and a repetition rate of 1 kHz was employed to ablate a Si wafer that was immersed in alcohol. An objective with a focusing length of 25 cm was used to focus the femtosecond laser beam on the Si wafer with a spot diameter of ≈40.0 µm. The as-prepared Si NSs were randomly dispersed on an Au/SiO_2 substrate. The morphology of the Si NSs was examined by using scanning electron microscopy (SEM).

Experimental Setup: The scattering spectra of Si NSs distributed on an Au/SiO_2 substrate were measured by using a conventional dark-field microscope (Observer A1, Zeiss). The Au/SiO_2 substrate was attached on a prism by using oil to ensure refractive index matching. Collimated white light was incident on the bottom surface of the Au film through the prism at a specified angle (see Figure 1). The polarization of the white light was adjusted by using a Glan prism. When the incidence angle was smaller than the critical angle, SPPs could not be excited on the surface of the Au film and the Si NS was excited only by the transmitted wave. For incidence angles larger than the critical one, the SPPs on the surface of the Au could be excited and the Si NS would be directly excited by the SPPs. In both cases, the scattering light of the Si NS was collected by using an objective with NA = 0.7 in the z-direction and directed to a spectrometer (SR500, Andor) for analysis. Meanwhile, the image of the scattering light was recorded by using a CCD (DS-Ri2, Nikon).

Fitting Model: Fano resonances originate from the interference between a superradiant mode and a subradiant one that spectrally and spatially overlap. In this work, we employed the formula developed by Gallinet and Martin to describe the lineshape of the Fano resonance, which is given as follows[38,45]

$$\sigma = \left\{\left[\left(\frac{\omega^2-\omega_a^2}{2W_a\omega_a}+q\right)^2+b\right]\Big/\left[\left(\frac{\omega^2-\omega_a^2}{2W_a\omega_a}\right)^2+1\right]\right\} \times \left\{a^2\Big/\left[\left(\frac{\omega^2-\omega_s^2}{2W_s\omega_s}\right)^2+1\right]\right\} \quad (1)$$

Seven resonance parameters, which are the central frequency ω_a, the spectral width W_a, the asymmetry parameter q, the maximum amplitude of the resonance a, the resonant frequency ω_s, the spectral width W_s, and an additional parameter b that quantifies the modulation damping of the resonance by intrinsic losses, were used in the fitting process.

Numerical Modeling: The scattering spectra of Si NSs were calculated by using the FDTD technique (commercial software developed by Lumerical Solution, Inc. (http://www.lumerical.com)). In the FDTD simulation, a nonuniform mesh size with the smallest meth size of 1 nm as well as a perfectly matched boundary condition was employed.

Supporting Information

Supporting Information is available from the Wiley Online Library or from the author.

Acknowledgements

J.X. and J.C. contributed equally to this work. S.L. acknowledges the financial support from the National Key Research and Development Program of China (no. 2016YFA0201002), the National Natural and Science Foundation of China (grant nos. 11674110 and 11874020), and the Natural Science Foundation of Guangdong Province, China (grant nos. 2016A030308010). The work of A.E.M. was supported by the Australian Research Council and UNSW Scientia Fellowship.

Conflict of Interest

The authors declare no conflict of interest.

Keywords

Fano resonances, high-refractive index materials, magnetic resonances, optical sensors, surface plasmon polaritons

Received: March 22, 2020
Revised: April 15, 2020
Published online:

[1] B. Luk'yanchuk, N. I. Zheludev, S. A. Maier, N. J. Halas, P. Nordlander, H. Giessen, C. T. Chong, *Nat. Mater.* **2010**, *9*, 707.
[2] U. Fano, *Phys. Rev.* **1961**, *124*, 1866.
[3] A. E. Miroshnichenko, S. Flach, Y. S. Kivshar, *Rev. Mod. Phys.* **2010**, *82*, 2257.
[4] M. Rahmani, B. Luk'yanchuk, M. Hong, *Laser Photonics Rev.* **2013**, *7*, 329.
[5] J. Yan, P. Liu, Z. Lin, H. Wang, H. Chen, C. Wang, G. Yang, *ACS Nano* **2015**, *9*, 2968.
[6] J. H. Yan, P. Liu, Z. Y. Lin, H. Wang, H. J. Chen, C. X. Wang, G. W. Yang, *Nat. Commun.* **2015**, *6*, 7042.
[7] M. F. Limonov, M. V. Rybin, A. N. Poddubny, Y. S. Kivshar, *Nat. Photonics* **2017**, *11*, 543.
[8] S. Lal, S. Link, N. J. Halas, *Nat. Photonics* **2007**, *1*, 641.
[9] J. N. Anker, W. P. Hall, O. Lyandres, N. C. Shah, J. Zhao, R. P. Van Duyne, *Nat. Mater.* **2008**, *7*, 442.
[10] F. Hao, Y. Sonnefraud, P. V. Dorpe, S. A. Maier, N. J. Halas, P. Nordlander, *Nano Lett.* **2008**, *8*, 3983.
[11] J. B. Lassiter, H. Sobhani, J. A. Fan, J. Kundu, F. Capasso, P. Nordlander, N. J. Halas, *Nano Lett.* **2010**, *10*, 3184.
[12] D. Dregely, M. Hentschel, H. Giessen, *ACS Nano* **2011**, *5*, 8202.
[13] K. M. Mayer, J. H. Hafner, *Chem. Rev.* **2011**,*111*, 3828.
[14] S. Zhang, K. Bao, N. J. Halas, H. Xu, P. Nordlander, *Nano Lett.* **2011**, *11*, 1657.
[15] Z. Fang, X. Zhu, *Adv. Mater.* **2013**, *25*, 3840.
[16] Z.-J. Yang, Z.-H. Hao, H.-Q. Lin, Q.-Q. Wang, *Nanoscale* **2014**, *6*, 4985.
[17] N. S. King, L. Liu, X. Yang, B. Cerjan, H. O. Everitt, P. Nordlander, N. J. Halas, *ACS Nano* **2015**, *9*, 10628.
[18] A. E. Miroshnichenko, Y. S. Kivshar, *Nano Lett.* **2012**, *12*, 6459.
[19] K. E. Chong, B. Hopkins, I. Staude, A. E. Miroshnichenko, J. Dominguez, M. Decker, D. N. Neshev, I. Brener, Y. S. Kivshar, *Small* **2014**, *10*, 1985.
[20] I. Staude, J. Schilling, *Nat. Photonics* **2017**, *11*, 274.
[21] C. Wu, N. Arju, G. Kelp, J. A. Fan, J. Dominguez, E. Gonzales, E. Tutuc, I. Brener, G. Shvets, *Nat. Commun.* **2014**, *5*, 3892.
[22] A. I. Kuznetsov, A. E. Miroshnichenko, M. L. Brongersma, Y. S. Kivshar, B. Lukâyanchuk, *Science* **2016**, *354*, aag2472.
[23] A. B. Evlyukhin, S. M. Novikov, U. Zywietz, R. L. Eriksen, C. Reinhardt, S. I. Bozhevolnyi, B. N. Chichkov, *Nano Lett.* **2012**, *12*, 3749.
[24] J. M. Geffrin, B. García-Cámara, R. Gómez-Medina, P. Albella, L. S. Froufe-Pérez, C. Eyraud, A. Litman, R. Vaillon, F. González, M. Nieto-Vesperinas, J. J. Sáenz, F. Moreno, *Nat. Commun.* **2012**, *3*, 1171.
[25] Y. H. Fu, A. I. Kuznetsov, A. E. Miroshnichenko, Y. F. Yu, B. Lukâyanchuk, *Nat. Commun.* **2013**, *4*, 1527.
[26] S. Jahani, Z. Jacob, *Nat. Nanotechnol.* **2016**, *11*, 23.
[27] E. Xifré-Pérez, L. Shi, U. Tuzer, R. Fenollosa, F. Ramiro-Manzano, R. Quidant, F. Meseguer, *ACS Nano* **2013**, *7*, 664.
[28] A. B. Evlyukhin, S. I. Bozhevolnyi, *Phys. Rev. B* **2015**, *92*, 245419.
[29] Z. Huang, J. Wang, Z. Liu, G. Xu, Y. Fan, H. Zhong, B. Cao, C. Wang, K. Xu, *J. Phys. Chem. C* **2015**, *119*, 28127.
[30] A. E. Miroshnichenko, A. B. Evlyukhin, Y. S. Kivshar, B. N. Chichkov, *ACS Photonics* **2015**, *2*, 1423.
[31] I. Sinev, I. Iorsh, A. Bogdanov, D. Permyakov, F. Komissarenko, I. Mukhin, A. Samusev, V. Valuckas, A. I. Kuznetsov, B. S. Luk'yanchuk, A. E. Miroshnichenko, Y. S. Kivshar, *Laser Photonics Rev.* **2016**, *10*, 799.
[32] H. Li, Y. Xu, J. Xiang, X. F. Li, C. Y. Zhang, S. L. Tie, S. Lan, *Nanoscale* **2016**, *8*, 18963.
[33] J. Xiang, Y. Xu, J.-D. Chen, S. Lan, *Nanophotonics* **2020**, *9*, 133.
[34] J. J. Mock, R. T. Hill, A. Degiron, S. Zauscher, A. Chilkoti, D. R. Smith, *Nano Lett.* **2008**, *8*, 2245.
[35] M. V. Rybin, A. B. Khanikaev, M. Inoue, K. B. Samusev, M. J. Steel, G. Yushin, M. F. Limonov, *Phys. Rev. Lett.* **2009**, *103*, 023901.
[36] F. Wen, J. Ye, N. Liu, P. Van Dorpe, P. Nordlander, N. J. Halas, *Nano Lett.* **2012**, *12*, 5020.
[37] Y. Huang, J. Yan, C. Ma, G. Yang, *Nanoscale Horiz.* **2019**, *4*, 148.
[38] M. Wang, A. Krasnok, T. Zhang, L. Scarabelli, H. Liu, Z. Wu, L. M. Liz-Marzán, M. Terrones, A. Alù, Y. Zheng, *Adv. Mater.* **2018**, *30*, 1705779.
[39] Y. Cui, J. Zhou, V. A. Tamma, W. Park, *ACS Nano* **2012**, *6*, 2385.
[40] S. Lepeshov, A. Krasnok, I. Mukhin, D. Zuev, A. Gudovskikh, V. Milichko, P. Belov, A. Miroshnichenko, *ACS Photonics* **2017**, *4*, 536.
[41] S. K. Ray, S. Chandel, A. K. Singh, A. Kumar, A. Mandal, S. Misra, P. Mitra, N. Ghosh, *ACS Nano* **2017**, *11*, 1641.
[42] S. Fan, *Appl. Phys. Lett.* **2002**, *80*, 908.
[43] B. Kim, K. J. Yoshihara, *Chem. Phys.* **1993**, *99*, 1433.
[44] J.-D. Chen, J. Xiang, S. Jiang, Q.-F. Dai, S.-L. Tie, S. Lan, *Nanoscale* **2018**, *10*, 9153.
[45] B. Gallinet, O. J. F. Martin, *ACS Nano* **2011**, *5*, 8999.
[46] A. Li, S. Isaacs, I. Abdulhalim, S. Li, *J. Phys. Chem. C* **2015**, *119*, 19382.

